Polymer Degradation and Stability 120 (2015) 122–134

Contents lists available at ScienceDirect

Polymer Degradation and Stability

journal homepage: www.elsevier.com/locate/polydegstab

Effect of carbon nanotubes on thermal pyrolysis of high density polyethylene and polypropylene

Omar Gutiérrez [a, b, *], Humberto Palza [a]

[a] Departamento de Ingeniería Química y Biotecnología, Facultad de Ciencias Físicas y Matemáticas, Universidad de Chile, Santiago, Chile
[b] Departamento de Ciencias Básicas, Facultad de Ciencias Exactas y Aplicadas, Instituto Tecnológico Metropolitano, Medellín, Colombia

ARTICLE INFO

Article history:
Received 13 February 2015
Received in revised form
29 May 2015
Accepted 17 June 2015
Available online 20 June 2015

Keywords:
Polyolefin pyrolysis
Thermal degradation
Thermogravimetric kinetic analysis
Carbon nanotube-polyethylene nanocomposites
Carbon nanotube-polypropylene nanocomposites

ABSTRACT

The goal of this work is to analyze the effect of carbon nanotubes (CNTs) on the pyrolysis of either high density polyethylene (PE) or polypropylene (PP) matrices by using both kinetic thermogravimetric analyses (TGA) under non-isothermal conditions and a fixed-bed reactor under isothermal conditions. Under non-isothermal conditions, CNTs increased the beginning of thermodegradation for both matrices with differences as high as 30 °C and 22 °C as compared with neat PP and PE, respectively. This enhanced thermal stability in PP based composites was associated with an increase in the apparent activation energy whereas in PE based composites lower pre-exponential factors associated with reduced conformational entropy, are responsible for the enhanced thermal stability. The thermodecomposition processes were studied by assuming geometrical contraction and nucleation models. The invariant pre-exponential factor and apparent activation energy obtained were quantified for each sample confirming that these values depended on the polymer matrix and concentration of CNTs. These invariant parameters were in good agreement with those obtained by isoconversional analyses allowing the prediction of the thermogravimetric behavior. Our findings clearly showed the strong effect of CNTs on the non-isothermal pyrolysis of polymer materials changing its kinetic and the activation energy. Results from isothermal pyrolysis (450 °C-40′) confirmed the thermal stability by the presence of CNTs as higher condensable (C_9–C_{40}) and lower gas (C_1–C_4) yields in PP-CNTs composites, and a higher amount of unreacted polymer and a lower both condensable and gas yields for PE-CNT, as compared with the pure matrix, were found.

© 2015 Elsevier Ltd. All rights reserved.

1. Introduction

The growing market of polymeric nanocomposites (PNCs) has raised a great interest thanks to the improvements in thermal, mechanical, electrical, and barrier properties, among others, that nanoparticles confer to the polymeric matrix at low loadings [1–11]. When PNCs were presented to the public for the first time in the 90s [12], a huge market opportunity was forecast and today a demand of c.a 3200 kTons with an approximated value of 15 billion US dollars is estimated in 2020 only for US [13]. Within PNCs, those based on polyolefins are of great importance covering more than 50% of the world demand of plastics, being polyethylene (PE) and polypropylene (PP) the main exponents [14,15]. Among nanoparticles with the highest demand, carbon nanotubes (CNTs) are considered as an unique reinforcement for polymers [16]. In particular, many studies have been carried out expanding the applications of PP and PE by adding CNT to improve the Young's modulus, tensile strength, gas permeability, flame retardancy, and electrical conductivity [8,11,17–21]. However, another important property to be analyzed is the thermal stability as often limits both processing and application of the these nanocomposites [22,23]. For instance, high density polyethylene (HDPE)/CNTs composites presented enhanced thermal stability as compared with pure HDPE using thermogravimetric analysis (TGA) under nitrogen atmosphere and non-isothermal conditions [23]. The weight loss of 5% for neat HDPE occurred at 431 °C while for composites with 3.0 wt% of CNT the same loss occurred at 459 °C. Bocchini et al. [24] found that CNTs dispersed in linear low density PE (LLDPE) delayed approximately 12 °C the thermal degradation respect to virgin matrix. This stabilization is due to both a thin film of CNTs net

* Corresponding author. Departamento de Ingeniería Química y Biotecnología, Facultad de Ciencias Físicas y Matemáticas, Universidad de Chile, Beauchef 850, Santiago, Chile.
E-mail address: omardariogutierrez@gmail.com (O. Gutiérrez).

http://dx.doi.org/10.1016/j.polymdegradstab.2015.06.014
0141-3910/© 2015 Elsevier Ltd. All rights reserved.

formed by migration at the polymer surface and an accumulation due to LLDPE volatilization. The same tendency was found in PP/CNTs nanocomposites exhibiting superior thermal stability as compared with neat PP under either nitrogen or air atmospheres [7]. Other studies found that, respect to pure PP, the addition of 0.5 and 1% wt of MWCNTs increases 16 °C and 34 °C respectively the onset of thermal degradation [25]. Moreover, Kashiwagi et al. [26] found a significant reduced flammability of PP at 1% wt of MWCNTs due to the formation of a network-structured floccule layer covering the entire sample surface. In general, several explanations for the improved thermal stability in the these systems are reported such as: 1) good matrix–nanotube interaction [21,25,27–29], 2) barrier effect of CNTs on the diffusion of degraded volatile components from polymeric matrix [21,25,30–32], 3) free radical scavenger effect of CNTs due their π-bonds [21,24,25,33], 4) the formation of a superficial protecting nanotube network which is destroyed when increasing the temperature up to a limit value [24,25,27], and 5) improvement of thermal conductivity in the polyolefinic-CNT nanocomposites which allows the spreading of heat uniformly within the composite [4,21,25].

The thermal behavior is also important considering the great consumption of plastic polymers, more than 300 million annual tons [34], demanding novel strategies for feedstock recycling such as the pyrolysis. This kind of chemical recycling has become one of the most attractive method for waste polymer treatment allowing the attenuation of their environmental impact besides the recovery and valorization of its degradation products [14,35–37]. Several studies have been carried out focusing on the products from pyrolysis of HDPE and PP and their potential industrial application [38–40]. For instance, if 1 kg of polyethylene is pyrolized in order to obtain a hypothetical mix of 10%-petroleum gas, 30%-gasoline, 40%-diesel and 20%-wax (residual oil), based on the calorific value of those commercial fuels, the net energy gained is estimated in 42 MJ/kg [41,42]. Assuming the great potential impact of polymer nanocomposites in the market, to understand the effect of nanoparticles on temperature and degradation processes is a very relevant topic in the context of chemical recycling processes.

To our knowledge, there are several reports about the effect of CNTs on the thermal properties of polyolefinic systems [43–49], but combines studies about both isothermal and non-isothermal (or dynamic) pyrolysis are barely found. In this sense, the goal of the present work is to analyze the effect of CNTs on the thermal pyrolysis of PP and HDPE, by means of two complementary approaches. The first one consisting in carried out non-isothermal (or dynamic) pyrolysis by means of thermogravimetric analysis, in order to get information related to the kinetics of the thermodecomposition reactions. This kinetic analysis gives information for the future design of industrial reactors and for in-use lifetime predictions [50–52]. The second one consisting in the analysis of the effect of CNTs on the products generated in a pyrolysis reactor under isothermal conditions in terms of their yield and composition.

2. Kinetic models for non-isothermal pyrolysis

Considering that the shape of thermogravimetric (TG) profiles does not change with time, we can assume that there is no constraints to apply dynamic data for kinetic investigations of a polymeric material [39]. The rate of reaction can be described therefore by using the following equations:

$$\frac{d\alpha}{dt} = K(T)f(\alpha) \tag{1}$$

$$\frac{d\alpha}{dt} = Ae^{-E_a/RT}f(\alpha) \tag{2}$$

where α is the reacted mass fraction at time t, $f(\alpha)$ is a function known as the differential form and it depends on the reaction mechanism adopting various expressions based on the specific model assumed, for instance: nucleation and nuclei growth, phase boundary reactions, diffusion, or order reactions, among others (see Table 1) [53–58]. $K(T)$ is the temperature-dependent rate constant, which has the Arrhenius form $Ae^{-E_a/RT}$, where Ea is the activation energy (kJ/mol), A is the pre-exponential factor of Arrhenius (s^{-1} or min^{-1}), R = gas constant (8.314 × 10^{-3} kJ mol^{-1} K^{-1}) and T is the absolute temperature (K).

If the TG run is carried out under dynamic conditions with a linear heating rate β, eq. (2) becomes:

$$\frac{d\alpha}{dT} = \frac{A}{\beta}e^{-E_a/RT}f(\alpha) \tag{3}$$

$$\int_0^{\alpha}\frac{d\alpha}{f(\alpha)} = \frac{A}{\beta}\int_{T_0}^{T_\alpha}e^{-E_a/RT}dT \tag{4}$$

By defining $g(\alpha) = \int_0^{\alpha}\frac{d\alpha}{f(\alpha)}$ and considering that α will be zero for $T < T_0$ (with T_0 being room temperature), it follows:

$$g(\alpha) = \frac{A}{\beta}\int_0^{T_\alpha}e^{-E_a/RT}dT \tag{5}$$

$g(\alpha)$ is known as the integral form and it depends on the reaction mechanisms. The term $\int_0^{T_\alpha}e^{-E_a/RT}dT$ is called temperature integral or Arrhenius integral, $I(Ea, T_\alpha)$, which has no analytic solution and numerical or approximate solutions are required [59,60].

The evaluations of the kinetic triplet "Ea, A, $f(\alpha)$" or "Ea, A, $g(\alpha)$" can be performed by using simultaneously two methods: (1) isoconversional methods (or model free methods), where the changes in TG data brought about by variation of heating rate allow to obtain Ea at a given conversion α, even when the functions $f(\alpha)$ and $g(\alpha)$ are not known; and (2) model fitting methods, where different mechanisms ($f(\alpha)$ or $g(\alpha)$) are proven until find the one that better describes the experimental data [51,61]. Keeping into account the ICTAC Kinetics Committee recommendations for thermal kinetic analyses [62,63], here we use two successive methods: (1) Isoconversional consisting in apply these methods to assess the apparent activation energy (Ea_{iso}) as a function of the conversion degree, and (2) Model fitting consisting in consider Ea_{iso} as a reference value meaning that these methods are carried out to assess the possible mechanism and corresponding kinetic parameters.

2.1. Isoconversional methods

The isoconversional procedures can be classified as linear or non-linear methods.

2.1.1. Linear isoconversional methods

The linear procedures can be differential (e.g. Friedman method) or integral (e.g. Flynn-Wall-Ozawa, Kissinger-Akahira-Sunose and Starink) methods. In the linear procedures such as those named Friedman (FR), Flynn-Wall-Ozawa (FWO), Kissinger-Akahira-

Table 1
Kinetic models for thermodecomposition reactions.

Model	Symbol	Differential form $f(\alpha)$	Integral form $g(\alpha)$
Nucleation models			
Power law	Pn (n = 2,3,4)	$n\alpha^{(n-1)/n}$	$\alpha^{1/n}$
Avrami–Erofeyev	An (n = 2,3,4)	$n(1-\alpha)[-\ln(1-\alpha)]^{(n-1)/n}$	$[-\ln(1-\alpha)]^{1/n}$
Geometrical contraction models			
Contracting area	R2	$2(1-\alpha)^{1/2}$	$1-(1-\alpha)^{1/2}$
Contracting volume	R3	$3(1-\alpha)^{2/3}$	$1-(1-\alpha)^{1/3}$
Diffusion models			
Uni-dimensional Diffusion	D1	$1/(2\alpha)$	α^2
Bi-dimensional Diffusion	D2	$-[1/\ln(1-\alpha)]$	$((1-\alpha)\ln(1-\alpha))+\alpha$
3-D Difusión-Jander	D3	$[3(1-\alpha)^{2/3}]/[\,2(1-(1-\alpha)^{1/3})\,]$	$(1-(1-\alpha)^{1/3})^2$
Ginstling-Brounshtein	D4	$3/[2((1-\alpha)^{-1/3}-1)]$	$1-(2/3)\alpha-(1-\alpha)^{2/3}$
Order-based models			
Zero order	F0, R1	1	α
First order	F1	$(1-\alpha)$	$-\ln(1-\alpha)$
n-order	Fn	$(1-\alpha)^n$	$[1/(n-1)][(1-\alpha)^{1-n}-1]$
Random scission $L=2$	L2	$2(\alpha^{-1/2}-\alpha)$	$-\ln(1-\alpha^{-1/2})$

Sunose (KAS) and Starink, represented at eqs. (6)–(9), respectively, for α = constant, the plot of the left hand side of these equations vs. *1/T*, obtained from thermograms recorded at several heating rates, should display a straight line whose slope allows an evaluation of the activation energy ($Ea_{\_l\_iso}$) [63–66].

$$ln\left(\frac{d\alpha}{dt}\right) = -\frac{E_a}{RT} + ln(Af(\alpha)) \tag{6}$$

$$ln\beta = -1,0518\frac{E_a}{RT} + C_2 \tag{7}$$

$$ln\frac{\beta}{T^2} = -\frac{E_a}{RT} + C_2 \tag{8}$$

$$ln\frac{\beta}{T^\kappa} = -C_1\frac{E_a}{RT} + C_2 \tag{9}$$

In the eq. (9) Starink suggests a suitable case for $\kappa = 1.92$ and $C_1 = 1.0008$ [65,66]. A comparison of the equations (7)–(9) shows that the eq. (9) includes FWO and KAS methods according to the values of κ, C_1 and C_2.

2.1.2. Non-linear isoconversional methods

In the non-linear procedures the activation energy ($Ea_{\_nl\_iso}$) is evaluated from a specific minimum condition [64]. An example of such approach is the method proposed by Vyazovkin [63,64,67,68], in which, for a set of *n* experiments carried out at different heating rates, the activation energy can be determined at any particular value of α by finding the value of activation energy ($Ea_{\_nl\_iso}$) for which the function

$$\Phi(E_\alpha) = \sum_{i=1}^{n}\sum_{j\neq i}^{n}\frac{I(E_\alpha, T_{\alpha,i})\beta_j}{I(E_\alpha, T_{\alpha,j})\beta_i} \tag{10}$$

Is a minimum. Then, the pre-exponential factor can be determined by minimizing the following objective function:

$$\Phi(A_\alpha) = \sum_{\substack{i\neq j\\ i<j}}^{n}\left|\frac{A_\alpha e^{-\frac{E_\alpha}{RT_{\alpha,i}}}}{\beta_i(d\alpha/dT)_{\alpha,i}} - \frac{A_\alpha e^{-\frac{E_\alpha}{RT_{\alpha,j}}}}{\beta_j(d\alpha/dT)_{\alpha,j}}\right| \tag{11}$$

Along all the performed heating rates.

2.2. Model fitting methods

As mentioned previously, a strategy to analyze the thermodegradation mechanisms consists in comparing the *Ea* obtained by isoconversional methods, $Ea_{\_iso}$, with *Ea* obtained for different evaluated mechanisms. Here, three model fitting methodologies have been considered: 1) Coats-Redfern (C-R), 2) master plots (MP) and 3) invariant kinetic parameters (IKP). C-R and MP allow to determine the kinetic triplet from only one curve at just one heating rate [69]. As a complement to this, IKP method allows to obtain a pre-exponential factor and activation energy independent on a given range of β, where these parameters are so-called invariant parameters [64,70].

2.2.1. Coats-Redfern (CR) method

The C-R method uses the integral [$g(\alpha)$] forms by means the relation:

$$ln\left[\frac{g(\alpha)}{T^2}\right] = ln\frac{AR}{\beta E_a} - \frac{E_a}{RT} \tag{12}$$

where the appropriate [$g(\alpha)$] mechanism will generate a straight line whose slope and intercept determine *A* and *Ea* parameters [66,71]. Additionally, if *Ea* is independent of α, this line should have a slope similar to $Ea_{\_iso}$ serving as a criterion for the selection of the most appropriate mechanism.

2.2.2. Master plots (MP) method

A MP is another theoretical reference curve depending on a kinetic model [$f(\alpha)$ or $g(\alpha)$] although generally it is independent of the kinetic parameters of the process. There are three classes of MP: 1) differential master plots, 2) integral master plots and 3) integro-differential master plots. In this work only differential (DMP) and integral (IMP) master plots are used because the DMP clearly distinguishes among different $f(\alpha)$ in the range $\alpha < 0.5$ while the IMP disperse for $\alpha > 0.5$ and therefore permits a straightforward identification [56]. With the integro-differential master plots otherwise it is not possible to distinguish between the mechanisms R3 and D3 nor between F1 and An mechanisms [56,72]. The MP can be obtained plotting a function $\Phi(\alpha)$ versus α, where $\Phi(\alpha)$ comes from the definition of MP [51,55,72]:

1) Differential master plots (DMP), if $\Phi(\alpha) = f(\alpha)/f(0.5)$.
2) Integral master plots (IMP), if $\Phi(\alpha) = g(\alpha)/g(0.5)$.

By giving values between 0 and 1 to α, these definitions allow to obtain a theoretical $\Phi(\alpha)$ function for every mechanism $f(\alpha)$ or $g(\alpha)$. It is also possible to express $\Phi(\alpha)$ functions in terms of experimental data such as:

1) For DMP:

$$\Phi(\alpha) = \frac{d\alpha/dt}{(d\alpha/dt)_{\alpha=0.5}} * \frac{e^{(E_a/RT)}}{e^{(E_a/RT_{\alpha=0.5})}} \quad (13)$$

2) For IMP:

$$\Phi(\alpha) = \frac{\left[\frac{e^{-E_a/RT}}{E_a/RT} * \pi(E_a/RT)\right]}{\left[\frac{e^{-E_a/RT}}{E_a/RT} * \pi(E_a/RT)\right]_{\alpha=0.5}} \quad (14)$$

The $\pi(E_a/RT)$ is an approximation of the temperature integral, $\frac{A}{\beta}\int_{T_0}^{T} e^{-E_a/RT}dT$ (see eq. (4)), based on the fourth rational expression of Senum and Yang, which give errors lower than 10^{-5}% for $E_a/RT > 20$ [55,72], condition satisfied in our experiments.

2.2.3. Invariant kinetic parameters (IKP) method

In order to apply this method for a given heterogeneous reaction, thermograms at several heating rates should be recorded. It is also needed to define a set of conversion functions that are not obliged to contain the true kinetic model. By starting from this set, for each heating rate the compensation parameters (α^*, β^*) are determined ($\ln A = \alpha^* + \beta^* Ea$). Then, the invariant activation parameters (A_{inv}, $Ea_{\_inv}$) can be evaluated using the supercorrelation relation:

$$\alpha^* = lnA_{inv} - \beta^* E_{a\_inv} \quad (15)$$

Using the values of A_{inv} and $Ea_{\_inv}$ and the rate equation, the numerical evaluation of $f_{\_inv}(\alpha)$ is performed by means of eq. (2). The eq. (15) is also important since it allows the calculation of pre-exponential factor values for activation energies determined through isoconversional methods [69]. It was pointed out that the values of $f_{\_inv}(\alpha)$ are especially affected by the errors in A_{inv} evaluation. Consequently, the values of $f_{\_inv}(\alpha)$ are proportional to the true (real) $f(\alpha)$ values. In order to discriminate the kinetic model, the shape of $f_{\_inv}(\alpha)$ vs. α curve could be compared with the shapes of $f(\alpha)$ vs. α curves corresponding to theoretical kinetic models. The true kinetic model can be obtained by successive application of IKP method and the criterion of independence of kinetic parameters on the heating rate. Additionally, it is important to highlight that Budrugeac [73] showed that diffusional models can deteriorate the linear correlation of both compensation and invariant parameters, increasing appreciably its standard deviation. Based on this, here the set of the reaction functions: Rn + An + Fn (Table 1) was considered.

3. Materials and methods

3.1. Raw materials

High density polyethylene, PE, (MFI = 8 g/10 min, supplied by Ipiranga Petroquimica), and isotactic-polypropylene, PP, (MFI = 3.6 g/10 min, supplied by Petroquim), were used as the polymeric matrices, and as nanofiller, multiwalled carbon nanotubes (supplied by Bayer Material Science AG). According to the supplier, the nanotubes have average external diameters of 13–16 nm approximately, lengths between 1 and 10 μm, and a carbon purity of 95% in weight. The PNCs were obtained by using a Brabender plasticorder internal mixer at 170 °C (for PE) and 190 °C (for PP) and a rotor rotation rate of 110 rpm. The PNCs were prepared with content of 0 (PE, PP), 3 (PE3CNT, PP3CNT) and 6 (PE6CNT, PP6CNT) wt.% of carbon nanotubes.

3.2. Thermal pyrolysis

The non-isothermal pyrolysis reactions were carried out by thermogravimetric analysis in a TG 209-F1 Libra equipment (NETZSCH) under dynamic heating conditions in an inert nitrogen atmosphere from room temperature up to 600 °C. Samples of specimens were 5–10 mg, the gas flow rate was 20 ml/min and the heating rates were of 5, 10, 15 and 20 K/min.

The isothermal pyrolysis reactions were carried out using a fixed bed reactor operating isothermally at 450 °C for 40 min, and N_2 (gas carrier) with a flow rate of 60 mL/min 0.5 g of PNC were loaded into the reactor. The emerging products during pyrolysis were collected by condensation in an expansion and in a jacketed collector in an ice-NaCl bath at −5 °C, and the gases were storaged in 1.5 L Tedlar bags. The products were classified as gases (C_1–C_4 range), condensables (C_9–C_{40} compounds) and "char + remaining polymer (RP)" (C_{40} < compounds). Here, char is the solid carbonaceous residue formed via thermal deconstruction and RP corresponds to wide spectrum of oligomers come from original polymeric sample. The yield of "char + RP" and condensables were obtained by weighting the reactor, expansion and collector before and after the runs, while the gases were estimated by mass balance. To assess the char/RP ratio present inside the reactor, these residues were submitted to TGA from 30 °C up to 600 °C in nitrogen atmosphere (pyrolytic TGA). After that, the residual mass was considered as char and the mass change as the corresponding RP.

Condensable samples were dissolved in hexane and analyzed utilizing a Shimadzu GC-2010 equipped with a manual injector and flame ionization detector (FID). The column RTX®-5 (30 m × 0.32 mm ID; 0.25 μm film thickness) was used with a nitrogen flow rate of 3.0 mL/min. The injector was set at 280 °C (split ratio of 50.0) and the temperature program began with a hold at 60 °C for 1 min followed by an increase at 12 °C/min to 300 °C, then 6 °C/min to 330 °C, which was held for 2 min the FID temperature was 340 °C and the injection volume was 1 μL. The gases were analyzed with a FID gas-chromatograph (Perkin Elmer Clarus 500) using a HP-Plot column (30 m × 0.32 mm ID; 0.25 μm film thickness) and flow rate of 20 mL/min of helium (carrier). The GC analysis started with injector at 250 °C and temperature program consisting of 45 °C held for 2.1 min, then a heating rate of 19.4 °C/min up to 170 °C and held for 5 min. The FID was at 250 °C and the injection volume was 50 μL.

4. Results and discussion

4.1. Non-isothermal behavior of nanocomposites

4.1.1. Thermogravimetric analyses

Derivative thermogravimetric (DTG) curves for PPCNT and PECNT nanocomposites are displayed in Fig. 1a showing a single step degradation for all systems, except neat PP, which has more than one process. Therefore, CNTs drastically affected the thermal degradation processes of the polymer matrix. In order to assess with more detail how many different processes are present? TG analyses at 1 K/min for all PP-CNT and PE-CNT samples were carried out (Fig. 1b) since this very low heating rate allows to detect overlapping processes more easily. Fig. 1b shows two peaks for neat

PP and just one peak for the other systems, suggesting at least two degradation processes in neat PP and corroborating one single process for the other samples. The temperature for 5% of weight loss ($T_{5\%}$) showed that CNTs acted as stabilizers for PP and PE matrices. $T_{5\%}$ (407 °C for neat PP) increased with the CNT content in 29 and 30 °C for PP3CNT and PP6CNT respectively. For PE based composites, the $T_{5\%}$ increased 14 and 22 °C for PE3CNT and PE6CNT respectively, as compared with pure PE ($T_{5\%}$ = 445 °C). In PP composites, these values did not change with the amount of filler probably due to agglomeration of CNTs [7,25]. The effect of the matrix on the thermal process is observed in Fig. 1c where the difference between temperatures at every α stage ($\Delta T = T_{nanocomposite}|_\alpha - T_{pure\ polymer}|_\alpha$) is plotted. ΔT diminished along the whole thermodecomposition for PPCNTs meanwhile for PECNTs this ΔT was initially high and turned constant (~13–15) for $\alpha > 0.4$. The tendency found in Fig. 1c can be explained assuming two competitive mechanisms during the thermodecomposition: 1) increased tortuosity as the polymer degradation increases the effective concentration of CNT; and 2) easy diffusivities of the low molecular weight species formed by the polymer degradation. The first mechanism means a larger effect of CNT as the reaction occurs meanwhile the second one means a lower effect of CNT. In PECNTs both mechanisms compensated each other explaining the almost constant behavior of ΔT during the reaction. However, in PP composites the first one seemed to be more relevant in the early stages of thermodegradation decreasing ΔT while the polymer reacts. This behavior agreed with the agglomeration phenomenon and also suggested a possible physical adsorption of polymeric chain and/or secondary radicals (generated throughout the pyrolysis) that decreases as the temperature increases [7,74]. This physisorption can be produced by Van der Waals interactions or mechanical interlocking as a consequence of polymer penetration into the nanotube bundles during melt mixing process [18,19].

4.1.2. Kinetics of thermodegradation

The apparent activation energies ($Ea_{\_I\_iso}$) evaluated at different conversion fractions (α) by using the linear isoconversional methods (equations (6)–(9)) are shown in Fig. 2. A similar dependence between *Ea* with α is displayed for Starink 1.92, FWO and KAS methods as all of them are integral methods that come from the same general expression (eq. (9)). However, these methods should be analyzed in the case where *Ea* is constant along the α as was pointed out by Budrugeac et al. [75]. In particular, there is an underestimation of *Ea* values by these integral isoconversional methods when *Ea* increases with α (as occurs in neat PP). Analogously, when *Ea* value decreases with α, these methods overestimate the true *Ea* values. However, 95%-confidence intervals calculated (see Fig. A in the supplementary material) with the standard deviation (from Fig. 2) and the corrected t-Student test for *Ea* estimation proposed by Vyazovkin and Sbirrazzuoli [76], only show a statistically significant difference between *Ea* values along α for neat PP. Therefore, *Ea* values obtained from FR analysis for neat PP are more reliable since it does not depend on the thermal history as integral methods do [75,77,78]. However, at conversions between 0.3 and 0.7, *Ea* is constant by the other methods. For the other samples *Ea* values from integral methods can be reliably used. Additionally, the variable *Ea* value for neat PP is coherent with their multiple processes (Fig. 1a y b) and one-step thermodegradation process for the rest of samples.

For alpha between 0.3 and 0.7, all methods present a constant value clearly pointing out that *Ea* tends to increase with CNTs content. This behavior is in agreement with Fig. 1 indicating their inhibitor effect on PP matrix. The same effect was reported under both inert [7,11,79] and oxidative conditions [80], and it was attributed to the radical-acceptor properties of CNTs [21,33,80]. An increased interfacial interactions between the CNTs and PP can further explain the higher *Ea* values for PPCNT nanocomposites

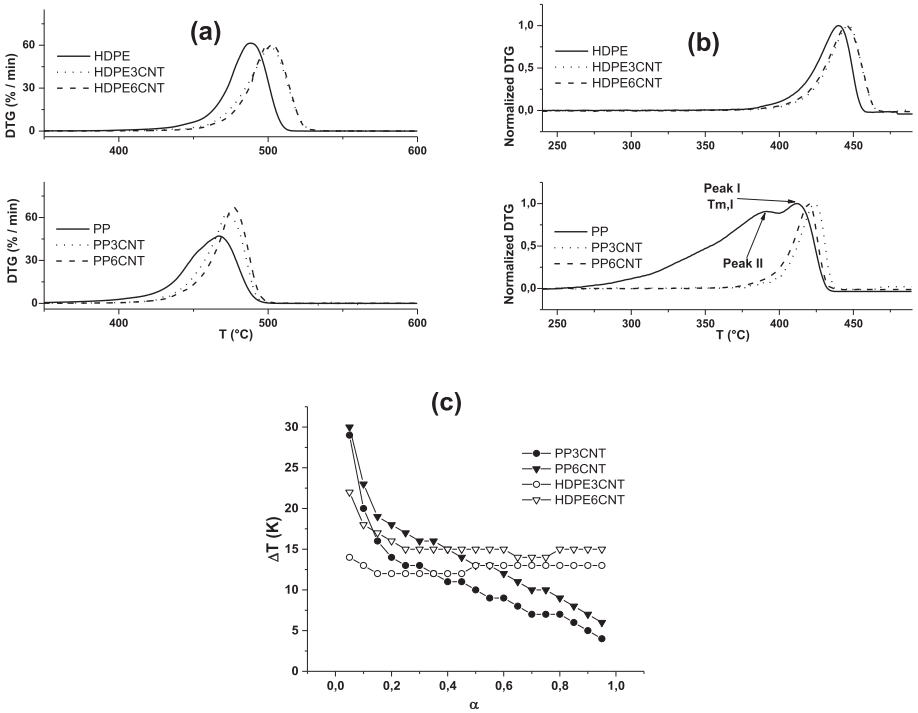

Fig. 1. Results obtained for PECNTs and PPCNTs. Thermodegradation rate (DTG) vs. temperature curves at: (a) $\beta = 20$ K/min, and (b) $\beta = 1$ K/min. (c) Thermal delay (ΔT) vs. alpha (at $\beta = 20$ K/min).

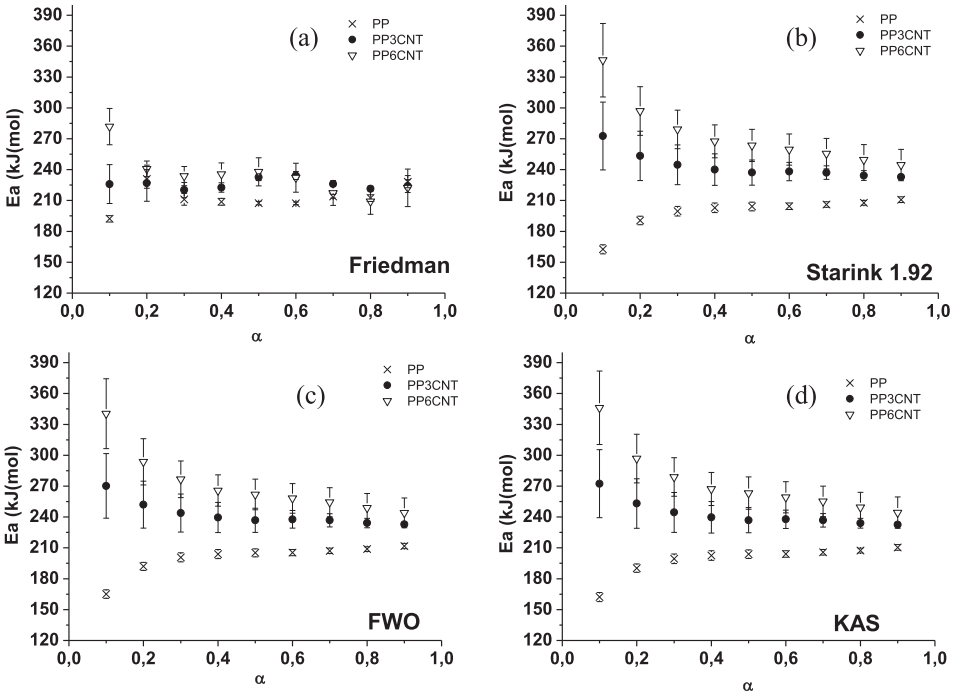

Fig. 2. *Ea* vs. α for PPCNT nanocomposites by methods of (a) Friedman. (b) Starink 1.92. (c) FWO. (d) KAS.

Table 2
$Ea_{\_iso}$ mean values of PPCNT and PECNT nanocomposites calculated for each isoconversional method.

		PP considering "one single process"	PP3CNT	PP6CNT	PE	PE3CNT	PE6CNT
Friedman's method	$Ea_{\_l\_iso}$ (kJ/mol)	215 ± 9	226 ± 5	229 ± 11	266 ± 16	229 ± 11	218 ± 7
Starink 1.92's method	$Ea_{\_l\_iso}$ (kJ/mol)	203 ± 6	240 ± 7	265 ± 17	263 ± 7	221 ± 5	184 ± 14
FWO's method	$Ea_{\_l\_iso}$ (kJ/mol)	204 ± 6	239 ± 6	263 ± 16	262 ± 6	221 ± 5	186 ± 13
KAS's method	$Ea_{\_l\_iso}$ (kJ/mol)	203 ± 6	239 ± 7	264 ± 17	263 ± 7	220 ± 5	183 ± 14
$Ea_{\_nl\_iso}$ value (kJ/mol)		203 ± 10	235 ± 5	250 ± 4	263 ± 4	226 ± 7	196 ± 5

[25,27]. This explanation also applies for our results based on ΔT as displayed in Fig. 1c.

Table 2 displays the $Ea_{\_l\_iso}$ mean value for each method taking into account values for $\alpha \geq 0.2$ (up to 0.9) in order to avoid the induction periods associated with the starting thermodegradation processes at the first stages [63]. In an attempt to refine the obtained $Ea_{\_l\_iso}$ values, the non-linear procedure (eq. (10)) was applied taking as initial guesses the *Ea* values obtained by all linear isoconversional methods in order to check the convergence to the optimized $Ea_{\_nl\_iso}$ values.

In the case of neat PP, as was before mentioned (see Fig. 1a y b), at least two processes are occurring. Keeping this in mind, the Table 2 lists preliminary *Ea* values under the approximation of one single thermodegradation process. These roughly *Ea* values are used only as initial guesses for the deconvolution and optimization of the mechanisms and its true activation kinetic parameters. Details of these procedures will be presented after the discussion of results for PP3CNT and PP6CNT samples.

By using the model fitting methods and taking the $Ea_{\_nl\_iso}$ values (Table 2) as reference, the Coats-Redfern (C-R) results (Eq. (12)) for the seventeen kinetic models examined and the four heating rates employed, indicated that the best mechanisms describing the thermodegradation of PP3CNT and PP6CNT, respectively, were: A2, and A2 at $\beta = 5$ K/min; R2, and R1-F0 at $\beta = 10$ K/min; R3, and A2 at $\beta = 15$ K/min; and L2, and R1-F0 at $\beta = 20$ K/min. For instance, the C-R results at $\beta = 20$ K/min for the 11 selected mechanisms are reported in Table 3. About C-R results, it is stressed tow facts: 1) the R^2 coefficient (Table 3) by itself was insufficient to determine the appropriate reaction mechanism as mechanisms with better R^2's and worst *Ea*-relative errors can simultaneously exist; and 2) their kinetic parameters are heavily dependant on the model selected for the fitting [63,81].

To supplement the mechanisms obtained by the C-R method, both the α versus T profile and the master plots were generated for PPCNT nanocomposites as displayed in Fig. 3a–c. Fig. 3a indicates a sigmoidal profiles for all PPCNT nanocomposites indicating that the R1-F0, D1 and P's type mechanisms must be discarded as they did not fit this tendency [53,63]. This agree with the master plots, for which D1 (unidimensional diffusion model) and P's (nucleation models) mechanisms have important deviations (see Table 3 and Fig. 3b and c) respect to experimental data. In this sense, the selection of the most probable mechanisms was based on both the residuals and relative errors between each mechanism and the experimental data, and the frequency of appearance of a mechanism for each heating rate. Table 4 shows the chosen mechanisms for PPCNT nanocomposites by means of C-R and master plots (MP) methods. We point out that the results obtained by C-R and MP methods remained the same trend for all heating rates. Here, for reasons of brevity, only the results at $\beta = 20$ K/min are shown in Table 3 and Fig. 3 and 6.

Table 4 shows that the thermodegradation of PPCNT nanocomposites can be described by means of the random scission (L2),

Table 3
Activation parameters (*Ea*, *A*) obtained by Coats-Redfern method for PPCNT and PECNT nanocomposites at every mechanism considered. (β = 20 K/min).

PP-peak 1					PP-peak 2				PP3CNT						PP6CNT					
Mechanism	Er	*Ea* (kJ/mol)	*ln A* (*A*/min^{-1})	R^2	Mechanism	Er	*Ea* (kJ/mol)	*ln A* (*A*/min^{-1})	R^2	Mechanism	Er	*Ea* (kJ/mol)	*ln A* (*A*/min^{-1})	R^2	Mechanism	Er	*Ea* (kJ/mol)	*ln A* (*A*/min^{-1})	R^2
F3	18	172 ± 8	27.4 ± 0.9	0.9699	A2	3	190 ± 6	30.4 ± 1.0	0.9495	L2	5	222 ± 5	36.2 ± 0.8	0.9780	R1_F0	2	254 ± 4	40.3 ± 0.6	0.9898
F2	22	162 ± 3	25.6 ± 0.5	0.9767	L2	30	256 ± 6	41.8 ± 1.0	0.9751	R1_F0	11	260 ± 5	41.4 ± 0.8	0.9827	L2	15	214 ± 7	34.6 ± 1.2	0.9476
F1	27	153 ± 6	23.9 ± 0.9	0.9828	P2	32	133 ± 9	20.6 ± 1.4	0.8323	R2	27	299 ± 3	47.3 ± 0.4	0.9964	R2	17	291 ± 4	45.9 ± 0.6	0.9909
R3	28	150 ± 7	22.3 ± 1.1	0.9847	A3	38	123 ± 4	19.1 ± 0.7	0.9461	A2	28	168 ± 2	26.7 ± 0.3	0.9939	R3	22	305 ± 5	47.9 ± 0.8	0.9879
R2	29	149 ± 6	22.4 ± 1.5	0.9856	R1_F0	41	278 ± 17	44.4 ± 2.8	0.8449	R3	34	314 ± 2	49.5 ± 0.3	0.9978	F1	35	337 ± 8	54.4 ± 1.2	0.9754
R1_F0	31	144 ± 3	22.3 ± 0.5	0.9882	A4	55	89 ± 3	13.4 ± 0.5	0.9423	P2	47	124 ± 3	19.0 ± 0.4	0.9808	A2	35	162 ± 4	25.7 ± 0.6	0.9737
D1	44	300 ± 6	47.6 ± 1.0	0.9890	P3	57	85 ± 6	12.4 ± 0.9	0.8182	F1	48	348 ± 4	56.5 ± 0.6	0.9942	P2	52	121 ± 2	18.5 ± 03	0.9888
D4	48	308 ± 10	46.8 ± 1.8	0.9868	P4	69	60 ± 4	8.2 ± 0.6	0.8025	P3	67	78 ± 2	11.4 ± 0.3	0.9787	P3	69	77 ± 1	11.0 ± 0.2	0.9876
L2	60	83 ± 2	12.5 ± 0.2	0.9726	F1	100	393 ± 13	63.7 ± 2.0	0.9527	P4	76	56 ± 1	7.4 ± 0.2	0.9761	P4	78	55 ± 1	7.1 ± 0.1	0.9861
PE					PE3CNT							PE6CNT								
Mechanism		Er	*Ea* (kJ/mol)	*A* (min^{-1})	R^2	Mechanism	Er	*Ea* (kJ/mol)	*A* (min^{-1})	R^2		Mechanism	Er	*Ea* (kJ/mol)	*A* (min^{-1})	R^2				
R2		2	267 ± 5	41.3 ± 0.8	0.9836	R1_F0	2	221 ± 6	33.7 ± 1.0	0.9629		A2	7	182 ± 3	27.9 ± 0.4	0.9909				
R3		7	280 ± 6	43.1 ± 0.9	0.9800	R2	12	253 ± 8	38.2 ± 1.2	0.9575		L2	23	241 ± 5	37.7 ± 0.8	0.9771				
R1_F0		11	234 ± 4	36.3 ± 0.7	0.9846	R3	17	265 ± 9	39.9 ± 1.3	0.9524		P2	32	134 ± 3	19.8 ± 0.5	0.9705				
F1		18	310 ± 8	49.1 ± 1.3	0.9663	L2	19	184 ± 9	28.7 ± 1.4	0.9006		A3	40	117 ± 2	17.4 ± 0.3	0.9903				
L2		26	196 ± 8	31.1 ± 1.2	0.9359	F1	29	292 ± 11	45.5 ± 1.7	0.9362		R1_F0	43	280 ± 7	43.0 ± 1.0	0.9732				
A2		44	149 ± 4	23.0 ± 0.6	0.9638	A2	38	140 ± 6	21.1 ± 0.8	0.9312		P3	57	85 ± 2	11.9 ± 0.3	0.9675				
P2		58	111 ± 2	16.4 ± 0.3	0.9829	P2	54	105 ± 3	15.1 ± 0.5	0.9588		A4	57	85 ± 1	12.0 ± 0.2	0.9897				
A3		64	95 ± 3	14.1 ± 0.4	0.961	P3	71	66 ± 2	8.6 ± 0.3	0.954		P4	69	61 ± 2	7.8 ± 0.2	0.9639				
A4		74	68 ± 2	9.5 ± 0.3	0.9578	F2	76	396 ± 25	62.7 ± 3.8	0.8461		F1	92	377 ± 5	58.8 ± 0.8	0.9914				

Er: Relative error of *Ea* value respect to $Ea_{\_nl\_iso}$ from Table 2.

geometrical contraction (R's) and nucleation (A's) models.

From these candidates, let us consider L2 first. This reaction model has been used successfully to describe the thermodecomposition (e.g. poly(butylene terephthalate)) by means of random scission reactions [57,58,82]. In this case, the expression deducted for $f(\alpha)$ is:

$$f(\alpha) = L(L-1)x(1-x)^{L-1} \tag{16}$$

where x and L are the fraction of bonds broken and the minimum length of the polymer that is not volatile, respectively. With the aim to implement the Eq. (16), a symbolic form for $f(\alpha)$ is neccesary and this happens when $L = 2$, being $f(\alpha) = 2(\alpha^{1/2} - \alpha)$ (expression listed in Table 1). Here, we want to illustrate that, even when the random scission processes can be fairly well fitted by L2 mechanism, this reaction model assumes that L is constant during the thermodegradation, which in not true considering the different length (C_1–C_{40}) of hydrocarbon products reported here in the Fig. 8 (PPCNT's) and 9 (PECNT's), and also reported in other investigations [83,84]. Even more, it is expected for non-isothermal pyrolyses that L increases with increasing temperature [85]. In this sense, we consider that the geometrical contraction (R's) and nucleation (A's) models are more consistent with the thermodegradation reactions of the samples. Finally, the L-type scission mechanisms have quite similar $f(\alpha)$ vs. α profiles as the Avrami (A's) models [57,58,64,82], which makes the data fit well even under L constant assumption.

Discarding L2 model, the previous methods showed that the thermodegradation of PPCNT nanocomposites could be fitted mainly by the mechanisms A and R. By further considering that [64,70]:

1) The activation parameters should satisfy the criterion of the independence on the heating rate, suggested by Perez-Maqueda et al.
2) The analytical form of $f(\alpha)$ leads to the same value of the pre-exponential factor, for various heating rates.
3) The true kinetic model implies an agreement between the activation energy obtained by means of an isoconversional method and that obtained by means of a differential or integral method, It is proposed that the thermodecomposition of PP3CNT and PP6CNT nanocomposites follows A2 nucleation mechanism along all the heating rates. Then, with the activation energies ($Ea_{\_nl\_iso}$ from Table 2.) and optimizing the objective function described by eq. (11), the pre-exponential factors were obtained and reported in Table 5.

On the other hand, for neat PP, taking into account the overlapping of peaks I and II in Fig. 1b, and in order to obtain the kinetic triplet, the kinetic parameters associated to named peak I was calculated (eq. 10 and 11) at different α values of the descending part starting from $T_{m,I}$ (Fig. 1b). The rising part of the peak I was not considered during the calculation due to partial overlapping at this side with the peak II. Later, with ($Ea_{\_nl\_iso}$, $A_{\_nl\_iso}$) parameters and CR and MP methodologies, R3 model was found as the most nearest mechanism. With this kinetic triplet, the TG shape of higher temperature peak I was then fitted and subtracted from the experimental TG curve of PP, to reveal the shape of the remaining part of the TG curve. On this remaining TG curve the same procedure was applied, and A2 kinetic model was found to be the better candidate. We consider the previous fitting as a preliminary deconvolution. Then, in order to obtain a more reliable kinetic triplets, a further optimization was carried out to determine the ϕ parameter that (for n heating rates) minimizes the function:

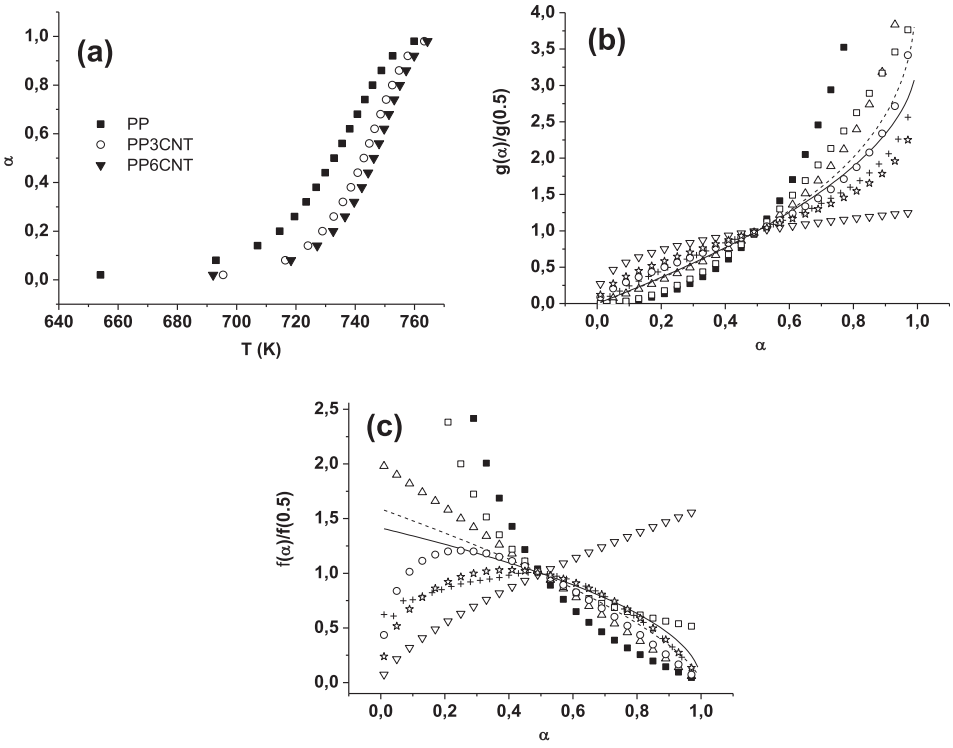

Fig. 3. Plots of (a) experimental α vs. temperature for PPCNT nanocomposites. Master plots for PP6CNT: (b) IMP, and (c) DMP. (All experimental data at $\beta = 20$ K/min). (+) Experimental data. (∇) P3. (Δ) F1. (■) D3. (□) D1. (┈┈) R3. (—) R2. (○) L2. (☆) A2.

$$\sum_{i=1}^{n}\left|\left(\frac{d\alpha}{dt}\right)_{\alpha,i}^{exp} - \varnothing\left(\frac{d\alpha}{dt}\right)_{\alpha,i}^{fitted-R3} - (1-\varnothing)\left(\frac{d\alpha}{dt}\right)_{\alpha,i}^{fitted-A2}\right|$$

In which, ϕ parameter is the effective contribution of R3 mechanism to the overall reaction rate $(d\alpha/dt)_{exp}$. This parameter was found to be 0.2, explaining the limited contribution of *Ea*(R3) to the nominal or global Ea values in Fig. 2. The final deconvolution results are summarized in Table 5, including the ϕ parameter within pre-exponential factors of Peaks 1 and 2 of neat PP. About the R3 mechanism obtained for peak 1 of PP, this is coherent with the R2 model reported by Aboulkas et al. [86], although due to the different methods and tests employed, existed differences with values reported in the literature [11,70,87,88]. For instance, Aboulkas reports *Ea* values of 179–188 kJ/mol considering only one single step of thermodegradation. These values are consistent with the nominal or apparent activation energy obtained from a kind of overlapping of *Ea*(R3) and *Ea*(A2) values listed here.

Comparing the mechanisms for PPCNT's respect pure PP, it is interesting to note that CNT's act as nucleating agents reducing the geometrical contraction-based thermodegradation processes. This nucleating activity has also been demonstrated during crystallization processes of CNT/PP composites [2,19,25,44], and here also plays a role during the thermodegradation. In agreement to this, other studies shown the potential of different nanoparticles as nucleating centers during thermodegradation reactions [7,89,90].

Table 4
Most probable mechanisms for PPCNT and PECNT nanocomposites by C-R and master-plots.

System	Method		
	Coats-Redfern	Master plots	
		IMP	DMP
PP-Peak 1	F's, R's	L2, R's	L2, A's, R's
PP-Peak 2	L2, A's	L2, A's	L2, A's
PP3CNT	L2, A's, R's	A's, R's	A's
PP6CNT	L2, A's, R's	A's, R's	A's
PE	R's	R's	R's, A's
PE3CNT	A's, R's	A's, R's	A's
PE6CNT	A's, R's	A's	A's

Table 5
Activation parameters for the thermal degradation of PPCNT and PECNT nanocomposites.

Sample	Optimized kinetic triplet			Invariant activation parameters			Lifetime values as a function of temperature $t_{5\%}$ (min)	
	Mechanism	$Ea_{\_nl\_iso}$ (kJ/mol)	$lnA_{\_nl\_iso}$ (A/min^{-1})	E_{a_inv} (kJ/mol)	$lnA_{\_inv}$ (A/min^{-1})	Rel_Dif[a] (%)	350 °C	400 °C
Peak 1-PP	R3	375 ± 9	31.5 ± 0.5	203 ± 8	32.1 ± 0.7	–	7.1E+01	7.5E+00
Peak 2-PP	A2	157 ± 11	24.7 ± 0.8	200 ± 10	31.7 ± 0.9			
PP3CNT	A2	235 ± 5	38.7 ± 0.8	261 ± 7	42.0 ± 0.9	11	7.4E+02	2.1E+01
PP6CNT	A2	250 ± 4	39.8 ± 0.6	222 ± 17	35.2 ± 0.7	−11	2.5E+03	4.0E+01
PE	R2	263 ± 4	40.6 ± 0.7	234 ± 8	36.6 ± 0.7	−11	2.4E+02	5.9E+00
PE3CNT	A2	226 ± 7	33.7 ± 1.0	225 ± 7	34.5 ± 1.0	−1	1.8E+03	6.5E+01
PE6CNT	A2	196 ± 5	31.3 ± 0.7	198 ± 14	30.2 ± 0.7	1	4.1E+02	3.2E+01

[a] Relative difference calculated as: 100*[$Ea_{\_inv}$ - $Ea_{\_nl\_iso}$]/$Ea_{\_nl\_iso}$; being $Ea_{\_nl\_iso}$ each mean value reported in Table 2.

Additionally, the change from two mechanisms (A2-R3) to just one (A2) due to CNTs agrees with behaviors observed in Fig. 1. This change in mechanism generates that while overall $d\alpha/dt$ decreases for neat PP, $d\alpha/dt$ increases for PP3CNT and PP6CNT (Fig. 1a and b) thus lowering ΔT in Fig. 1c. This is attributed to an initial induction time due to the formation of discrete nuclei (degradation centers), followed by a sudden acceleration of the reaction as it extends into the rest of the matrix [89].

In order to obtain both invariant (on heating rates) kinetic parameters and the numeric evaluation of $f_{\_inv}(\alpha)$, the IKP method was carried out (the compensation effect parameters obtained are listed in Table A in the supplementary material). Applying the supercorrelation (eq. (15)) the invariant activation parameters were obtained (see Table 5). From this table it can be seen that $Ea_{\_inv}$ values were within the Ea range at Fig. 2 and were in good agreement with the $Ea_{\_iso}$ mean values obtained by the both linear and non-linear isoconversional methods.

Fig. 4 Shows the experimental and simulated TG curves for PPCNT nanocomposites using the $f_{\_inv}(\alpha)$ obtained by the invariant kinetic parameters listed in Table 5. From this figure, we can state that IKP method gives a reliable predictions.

In addition to the previous results about thermal stability, a major application of TG and DTG kinetic analysis is to predict the maximum usable temperature, the optimum processing temperature regions, and estimated lifetime of polymers [51]. The lifetime is considered when 5% weight loss or 5% conversion ($t_{5\%}$) is reached from an isothermal TGA experiment [91], and can be calculated starting from eq. (5) as follows:

$$g(\alpha) = \frac{A}{\beta}\int_0^{T_\alpha} e^{-E_a/RT}dT \tag{5}$$

Under isothermal conditions,

$$g(\alpha) = Ae^{-E_a/RT}t \tag{5'}$$

$$t = \frac{Ae^{-E_a/RT}}{g(\alpha)} \tag{5''}$$

Considering the kinetic triplet in Table 5 $t_{5\%}$ can be calculated. For pure PP it was found that its thermodegradation process can be described by R3 and A2 mechanisms occurring simultaneously. In this case:

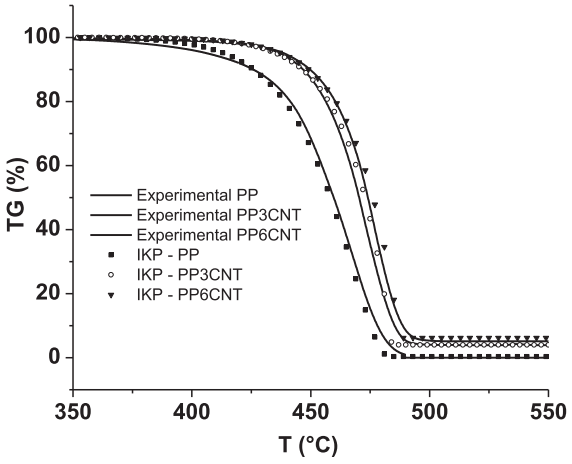

Fig. 4. Experimental and simulated TG curves for PPCNT nanocomposites.

$$\alpha_{global} = \frac{(\alpha_{A2} + \alpha_{R3})}{2} \tag{17}$$

Being α_{global} the total mass loss, and α_{A2}, α_{R3} the partial mass losses associated to A2 and R3 mechanisms respectively. Considering eq. (5′) and the integral form ($g(\alpha)$) of A2 and R3 mechanisms, an expression for α_{global} is obtained:

$$\alpha_{global} = \frac{\left(2 - (1 - k_{R3}t)^3 - e^{-k_{A2}^2 t^2}\right)}{2} \tag{18}$$

And with this equation, $t_{5\%}$ can be calculated for pure PP. Table 5 lists the $t_{5\%}$ obtained at simulated isothermal treatments of 300, 350 and 400 °C. From these, it can be seen the CNT's enhancing the thermal stability of PP and PE matrices, as well as PP degrades faster than PE, as experimentally occur, which can be explained observing that PP presents a tertiary carbon in the monomer unit likely to be attacked. This decreases the stability of PP as compared to PE [92–94].

Regarding PE samples, the apparent activation energy measured for the pure polymer, 263 kJ/mol, from Table 2 and Fig. 5, agreed with previous values of 245–260 kJ/mol reported by Chrissafis et al. [7,11]. However, for PECNT nanocomposites Chrissafis et al. found a 5% increase of Ea values meanwhile our results indicate lower values. This tendency implied that in our case the steric factor was a key effect for enhanced thermal stability. Under this context, polymer movement was sterically restricted by CNTs implying lower pre-exponential factors and consequently enhancing the thermal degradation. This phenomenon further can explain both the constant delay ΔT observed along α in Fig. 1a and its increase with CNT load.

For pure PE, the isoconversional, C-R and master plots methods (Fig. 6, Table 3) showed that R2 mechanism is the most probable. By applying these analyses to PE3CNT and PE6CNT, the A2 mechanism was chosen for both composites. Chrissafis et al. [11] proposed two consecutive reactions described by a n-order autocatalytic mechanisms: $f(\alpha) = (1\text{-}\alpha)^n(1+K_{cat}X)$ in order to explain the Ea values between 140 and 270 kJ/mol along the thermodecomposition of PECNTs. Certainly, this autocatalytic model satisfied the sigmoidal profile observed in Fig. 6a, but in our case Ea values were constant considering the 95% confidence intervals calculated with the corrected t-Studdent test (see Fig. A in the supplementary material). The presence of one single mechanism in both neat PE and PECNTs, unlike PP and PPCNTs, is consistent with the constant ΔT observed in Fig. 1c for $\alpha > 0.2$. The higher ΔT values at $\alpha < 0.2$ are attributed to the nucleation period mentioned before for PPCNTs.

In order to apply the IKP method on data from Fig. 6a, the invariant activation parameters were obtained for PECNT samples (see Table 5). In this case, we discarded the R1-F0, D1 and P's type mechanisms and employed the same set of reaction functions: R, A and F mechanisms. Table 5 shows that $Ea_{\_inv}$ values were near to $Ea_{\_iso}$ mean values obtained by isoconversional methods confirming their validity. With the invariant activation kinetic parameters, the TG curves for PECNT nanocomposites were successfully represented in Fig. 7. Also for PECNT systems, $t_{5\%}$ (Table 5) shows enhanced thermal stability respect to neat PE.

Both PPCNT and PECNT nanocomposites share the same kind of mechanisms although CNTs affects the activation kinetic parameters in different ways. From the invariant kinetic parameters (Table 5), the $A_{\_inv}$ values for PPCNTs were similar and the thermal stability was explained by the higher $Ea_{\_inv}$ values, which is associated with the adsorption of different species during the pyrolysis [25,27]. On the other hand, for PECNT nanocomposites lower values of $Ea_{\_inv}$ were obtained as compared with the pure matrix with the $A_{\_inv}$ parameters explaining the enhanced thermal stability.

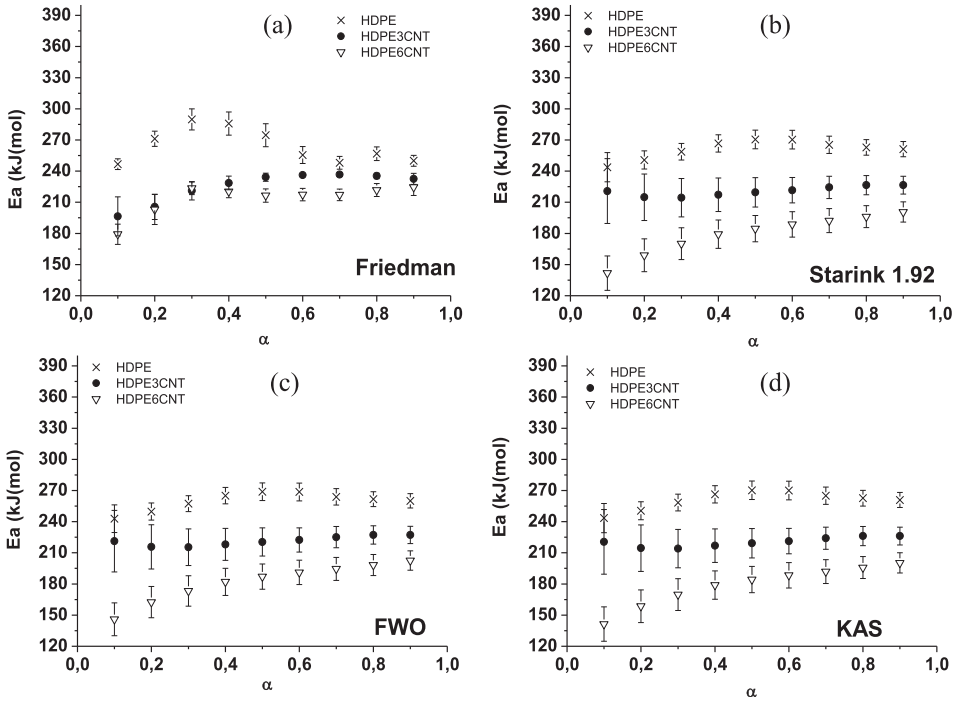

Fig. 5. *Ea* vs. α for PECNT nanocomposites by methods of (a) Friedman. (b) Starink 1.92. (c) FWO. (d) KAS.

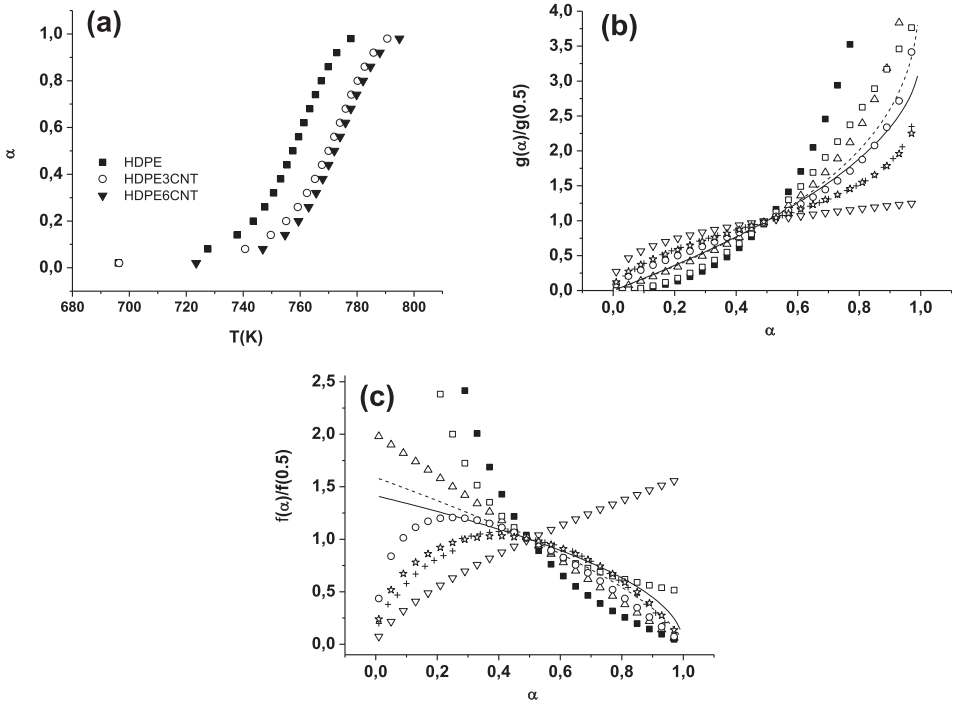

Fig. 6. Plots of (a) experimental α vs. temperature for PECNT nanocomposites. Master plots for PE: (b) IMP, and (c) DMP. (All experimental data at $\beta = 20$ K/min). (+) Experimental data. (∇) P3. (Δ) F1. (■) D3. (□) D1. (····) R3. (—) R2. (○) L2. (☆) A2.

According to Eyring's theory for the transition state (activated complex), the pre-exponential factor A in the Arrhenius equation contains an entropy term expressed by Refs. [95,96]:

$$A = \frac{\chi e^{n} k_B T}{h} exp\left(\frac{\Delta S^{\#}}{R}\right) \tag{19}$$

where χ is the transmission coefficient which accounts for the possibility of the activated complex to decompose with the formation of the end products of the reaction; n is the molecularity (or order) of the reaction; k_B is the Boltzmann constant; h is the Planck constant and $\Delta S^{\#}$ is the change of entropy of the activated complex from the reagents. In this sense, the presence of the particle surface can reduce the conformational freedom, and thus the entropy, of the polymeric chains due to excluded volume interactions [45], lowering the lnA_{inv} values from 36.6 $ln(min^{-1})$ (neat PE) to 34.5

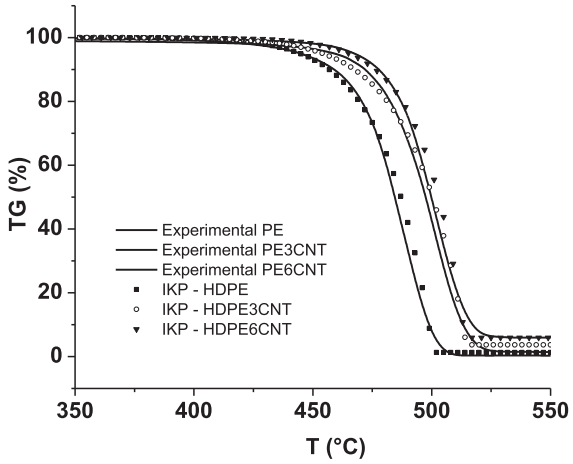

Fig. 7. Experimental and simulated TG curves for PECNT nanocomposites.

$ln(min^{-1})$ and 30.2 $ln(min^{-1})$ for PE3CNT and PE6CNT respectively. This important reduction (1-2 orders of magnitude) in the $A_{\_inv}$ values corresponds to reduction of $\Delta S^{\#}$ values for PE3CNT and PE6CNT classifying the thermodegradation of these last ones as slow as compared to pure PE. Many factors, such as intrinsic features of polymeric matrix/nanofiller, can be responsible of the differences between the thermal stability tendency of PPCNT and PECNT nanocomposites.

4.2. Isothermal behavior of nanocomposites

The operation temperature for isothermal pyrolysis was selected at 450 °C because under this condition (see Fig. 1a) the moderate thermodegradation rate favored the assessment the effect of CNTs. Fig. 8a shows the effect of CNTs on the fraction distribution of products coming from the PP pyrolysis under isothermal conditions. By adding CNTs to PP matrix, both a higher condensable and a lower gas yields as compared with the pure matrix were mainly observed. This tendency toward heavier hydrocarbons clearly evidenced a reduced cracking level due to the presence of CNTs confirming the enhanced thermal stability of composites under non-isothermal conditions. The reason of this tendency can be related with the energy needed to separate from CNTs surface the adsorbed products formed during the pyrolysis, oligomers or condensables [30]. Therefore, part of the heat flow should overcome this energetic barrier following an evaporation process rather than a cracking process.

By using pyrolytic TGA on "char + RP" ("char + remaining polymer") fraction, a composition of practically 0% of char for all samples was found, implying RP yields of 8%, 5% and 7% for PP, PP3CNT and PP6CNT respectively, and indicating that CNTs did not promote char formation. The selectivity to a certain specie *i* (hydrocarbon) in a fraction *j* (condensable or gas) was defined as: $[(\text{Chromatographic area})_i/(\text{Total chromatographic area})_j]$ x $(\text{Yield})_j$. This selectivity as displayed in Fig. 8(b and c) shows that the presence of CNTs produced a lower generation of C_3's gases and a higher presence of C_9–C_{15} and C_{18}–C_{23} hydrocarbons in PP pyrolysis. This confirmed the lower thermal cracking in composites as these C_9–C_{15} and C_{18}–C_{23} compounds did not suffer cracking. Finally, we can state that CNTs promote a larger production of diesel (C_9–C_{27}) type liquid fuel. This range of hydrocarbons justifies the previous discussion about L2 random scission mechanism.

Fig. 9a shows a much higher quantity of "char + RP″ in PE samples than in PP samples confirming the relevance of the polymer matrix in the pyrolysis. The TGA carried out on the residual solids of PECNTs showed a yield of 2%-char and 28%-RP for PE, 4%-

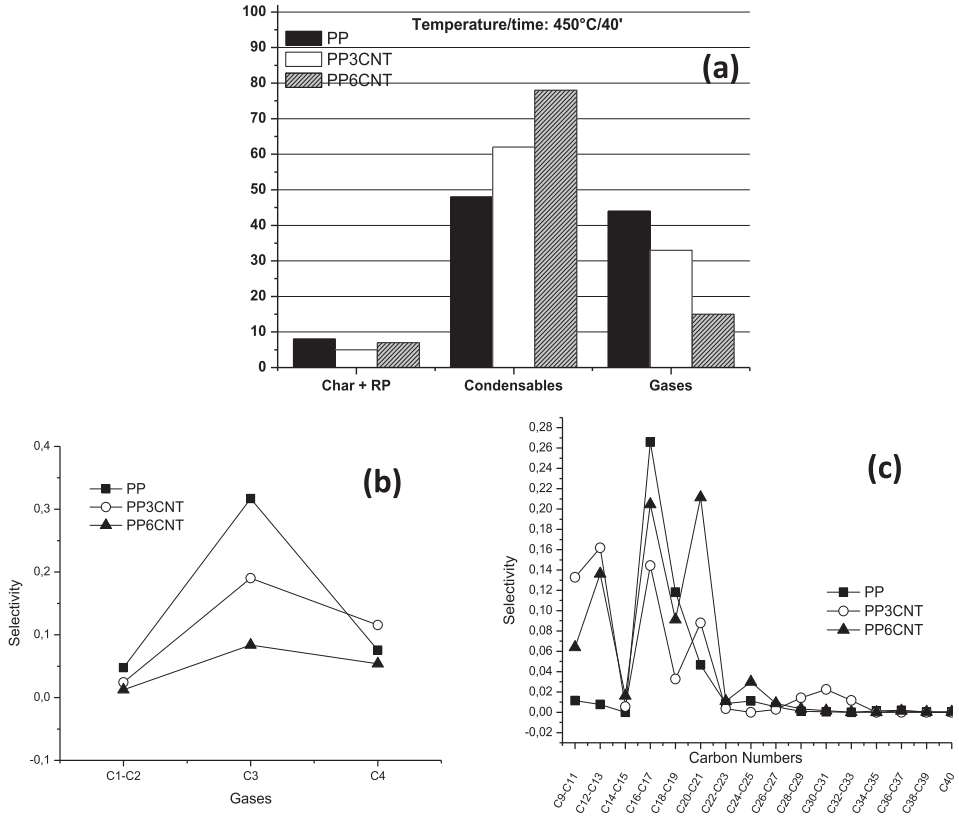

Fig. 8. Isothermal pyrolysis (450 °C-40′) of PPCNT nanocomposites. (a) Yield fraction distributions. Carbon number distributions of: (b) Gases. (c) Condensables.

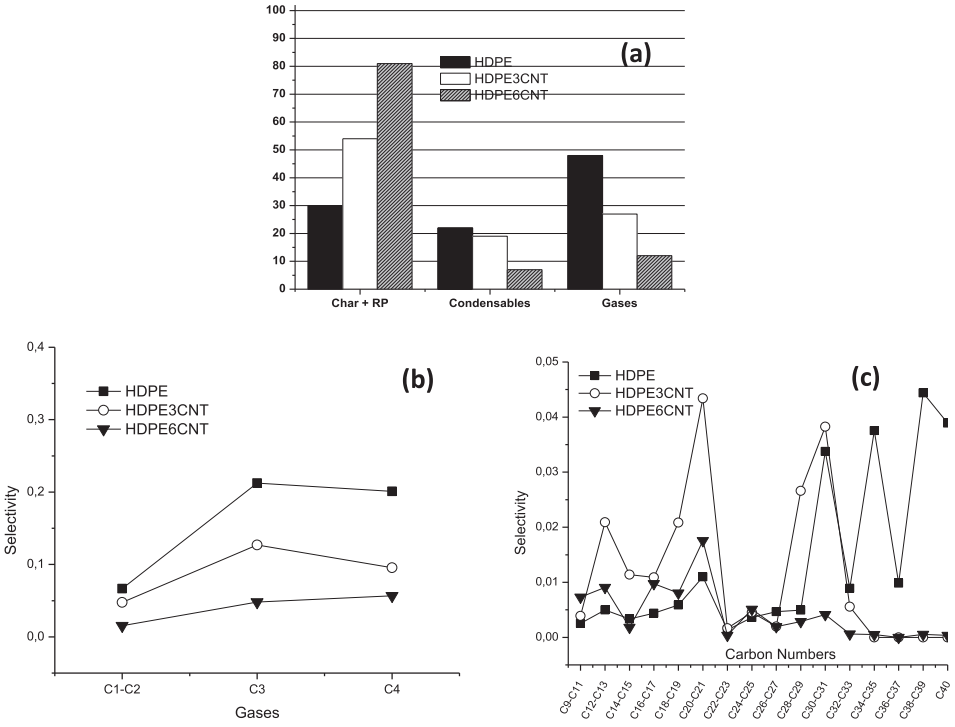

Fig. 9. Isothermal pyrolysis (450 °C-40′) of PECNT nanocomposites. (a) Yield fraction distributions. Carbon number distributions of: (b) Gases. (c) Condensables.

char and 50%-RP for PE3CNT, and 4%-char, 77%-RP for PE6CNT. From Fig. 9a was further concluded a lower conversion in PECNTs than PPCNTs in terms of RP thermo-degraded, being in agreement with $T_{5\%}$ values reported in section *4.1.1*. The RP values indicated that for PECNTs the reduced mobility of polymer chains can induce branching and cross-linking reactions. These reactions usually take place between ~200 °C and 290 °C, and above that temperatures PE begins to decompose reducing its molecular weight [93]. During these decomposition stages, oligomers with wide carbon number distributions are generated contributing to the RP formation. Additionally, the reduced mobility of chains in PECNTs can promote the propagation of scissions via intramolecular hydrogen transfer reactions increasing the yielding of gases as observed in Fig. 9a. These processes associated with branching and cross-linking reactions are not present in PP matrices.

Regarding the mechanisms for the production of the C_1–C_{40} compounds displayed in Figs. 8 and 9b and c, both intramolecular hydrogen transfer (IHT) and β-scission reactions are reported as the main processes involved [14,83]. For instance, in PP's pyrolysis primary radicals can produce propane and secondary radicals meaning the production of pentane and 2 methyl-1-pentene [93], as detected by GC–MS (results not shown). In the case of PE, the β-scission reactions produce 1-hexene and propene by means of IHT 1,5 reactions. However, IHT 1,5 is just one of the IHT 1,X reactions associated with shift or backbiting reactions where X typically can take values larger than 3 depending on the relative extent of the reaction [39]. The IHT 1,5 particularly is very favorable geometrically as the transition state is a six membered ring [50]. These reactions playing a crucial role because of a primary radical created during initiation or propagation stages can undergo IHT producing secondary macro-radical and thus increasing the free-radical stability. This new secondary radical will undergo either β-scission or multiple IHT 1,5 increasing products associated with 6, 10, 14, 22 alkenes and 3, 7, 11, 15 alkanes [39,83,92] as those displayed in Figs. 8c and 9c.

5. Conclusions

CNTs act as thermal stabilizers during pyrolyzes of PE and PP nanocomposites increasing for instance the onset for thermodegradation under non-isothermal conditions and reducing the extent of cracking level under isothermal condition. The specific mechanisms for this stabilization highly depends on the matrix characteristics. Geometrical contraction (R) and nucleation (A) mechanisms explains the pyrolysis reactions for all nanocomposites as measured by the isoconversional and model fitting methods. PPCNT composites presented larger apparent activation energy as compared with pure PP matrix associated with the stabilization of physisorbed radicals. In PECNTs, lower pre-exponential factor values were obtained as compared with PE matrix due to the reduced entropy generated by CNT delaying the themodecomposition.

The invariant kinetic parameters obtained with the IKP method were validated by two independent methods. Our results support that even complex thermodegradation processes such as those associated with the presence of nanofiller can be studied by invariant kinetic parameters toward chemical recycling processes design.

Acknowledgments

The authors acknowledge to:

Comisión Nacional de Investigación Científica y Tecnológica (Conicyt), for financial support of doctoral studies.

Fundación COPEC-UC, project UC9C006 for the financial support of this research.

Appendix A. Supplementary data

Supplementary data related to this article can be found at http://dx.doi.org/10.1016/j.polymdegradstab.2015.06.014.

References

[1] P. Song, Z. Cao, Y. Cai, L. Zhao, Z. Fang, S. Fu, Polym. Guildf. 52 (2011) 4001.
[2] Y. Jia, K. Peng, X. Gong, Z. Zhang, Int. J. Plast. 27 (2011) 1239.
[3] T.V. Duncan, J. Colloid Interface Sci. 363 (2011) 1.
[4] Z. Han, A. Fina, Prog. Polym. Sci. 36 (2011) 914.
[5] M. Zhang, U. Sundararaj, Macromol. Mater. Eng. 291 (2006) 697.
[6] E. Moncada, R. Quijada, I. Lieberwirth, M. Yazdani-Pedram, Macromol. Chem. Phys. 207 (2006) 1376.
[7] K. Chrissafis, D. Bikiaris, Thermochim. Acta 523 (2011) 1.
[8] B.-X. Yang, J.-H. Shi, K.P. Pramoda, S.H. Goh, Compos. Sci. Technol. 68 (2008) 2490.
[9] X. Peng, E. Ding, F. Xue, Appl. Surf. Sci. 258 (2012) 6564.
[10] A. Funck, W. Kaminsky, Compos. Sci. Technol. 67 (2007) 906.
[11] K. Chrissafis, K.M. Paraskevopoulos, I. Tsiaoussis, D. Bikiaris, J. Appl. Polym. Sci. 114 (2009) 1606–1618.
[12] R. Pfaendner, Polym. Degrad. Stab. 95 (2010) 369.
[13] U.S. Marketwire, Polym. Nanocomposites Demand Exceed 7 Billion Pounds 2020 (2006) 1.
[14] S.M. Al-Salem, P. Lettieri, J. Baeyens, Prog. Energy Combust. Sci. 36 (2010) 103.
[15] E. Butler, G. Devlin, K. McDonnell, Waste Biomass Valorization 2 (2011) 227.
[16] M. Razavi-Nouri, M. Ghorbanzadeh-Ahangari, A. Fereidoon, M. Jahanshahi, Polym. Test. 28 (2009) 46.
[17] T. McNally, P. Pötschke, P. Halley, M. Murphy, D. Martin, S.E.J. Bell, G.P. Brennan, D. Bein, P. Lemoine, J.P. Quinn, Polym. Guildf. 46 (2005) 8222.
[18] M. Pöllänen, S. Pirinen, M. Suvanto, T.T. Pakkanen, Compos. Sci. Technol. 71 (2011) 1353.
[19] E. Logakis, E. Pollatos, C. Pandis, V. Peoglos, I. Zuburtikudis, C.G. Delides, a Vatalis, M. Gjoka, E. Syskakis, K. Viras, P. Pissis, Compos. Sci. Technol. 70 (2010) 328.
[20] A. Rahman, I. Ali, S.M. Al Zahrani, R.H. Eleithy, Nano 06 (2011) 185.
[21] M. Moniruzzaman, K.I. Winey, Macromolecules 39 (2006) 5194.
[22] H. Palza, R. Vergara, P. Zapata, Compos. Sci. Technol. 71 (2011) 535.
[23] M. El Achaby, a Qaiss, Mater Des 44 (2013) 81.
[24] S. Bocchini, A. Frache, G. Camino, M. Claes, Eur. Polym. J. 43 (2007) 3222.
[25] D. Bikiaris, Mater. Basel 3 (2010) 2884.
[26] T. Kashiwagi, E. Grulke, J. Hilding, K. Groth, R. Harris, K. Butler, J. Shields, S. Kharchenko, J. Douglas, Polym. Guildf. 45 (2004) 4227.
[27] B.B.þ. Marosf, A. Szabó, G. Marosi, D. Tabuani, G. Camino, S. Pagliari, J. Therm. Anal. Calorim. 86 (2006) 669.
[28] M. Wong, M. Paramsothy, X.J. Xu, Y. Ren, S. Li, K. Liao, Polym. Guildf. 44 (2003) 7757.
[29] L.Y. Jiang, Y. Huang, H. Jiang, G. Ravichandran, H. Gao, K.C. Hwang, B. Liu, J. Mech, Phys. Solids 54 (2006) 2436.
[30] K. Hassan, M. Rahman, F. Mina, M. Remanul, A. Gafur, A. Begum, Compos. Part A 52 (2013) 70.
[31] A.D. Drozdov, Eur. Polym. J. 43 (2007) 1681.
[32] H. Palza, R. Vergara, P. Zapata, Macromol. Mater. Eng. 295 (2010) 899.
[33] J. Kim, Y.P. Seo, Y. Seo, S.M. Hong, 766 (2011) 761.
[34] S. Kumar, A.K. Panda, R.K. Singh, Resour. Conserv. Recycl 55 (2011) 893.
[35] Y.-H. Lin, M.-H. Yang, Appl. Catal. A Gen. 328 (2007) 132.
[36] S.M. Al-Salem, P. Lettieri, J. Baeyens, Waste Manag. 29 (2009) 2625.
[37] J.F. Mastral, C. Berrueco, M. Gea, J. Ceamanos, Polym. Degrad. Stab. 91 (2006) 3330.
[38] B. Singh, N. Sharma, Polym. Degrad. Stab. 93 (2008) 561.
[39] K. Pielichowski, J. Njuguna, Thermal Degradation of Polymeric Materials, First, Shawbury, Shrewsbury, Shropshire, SY4 4NR, UK ©2005, 2005.
[40] Y.-H. Lin, M.-H. Yang, J. Anal, Appl. Pyrolysis 83 (2008) 101.
[41] J. Scheirs, W. Kaminsky, Feedstock Recycling and Pyrolysis of Waste Plastics: Converting Waste Plastics into Diesel and Other Fuels, John Wiley & Sons Ltd, The Atrium, Southern Gate, Chichester, West Sussex PO19 8SQ, UK, 2006.
[42] G. Feng, Pyrolysis of Waste Plastics into Fuels, University of Canterbury, 2010.
[43] M. Chipara, R. Wilkins, E.V. Barrera, M.D. Chipara, Compos. Interfaces 17 (2010) 625.
[44] D. Xu, Z. Wang, Polym. Guildf. 49 (2008) 330.
[45] I. Szleifer, R. Yerushalmi-rozen, Polym. Guildf. 46 (2005) 7803.
[46] V. Goodarzi, A. Shadakhtar, M. Sirousazar, M. Mortazavi, J. Reinf, Plast. Compos 32 (2013) 846.
[47] R. Kotsilkova, E. Ivanov, E. Krusteva, C. Silvestre, S. Cimmino, D. Duraccio, J. Appl, Polym. Sci. 115 (2010) 3576.
[48] B. Dittrich, K.-A. Wartig, D. Hofmann, R. Mülhaupt, B. Schartel, Polym. Degrad. Stab. 98 (2013) 1495.
[49] B. Yuan, C. Bao, L. Song, N. Hong, K. Meow, Y. Hu, Chem. Eng. J. 237 (2014) 411.
[50] J.D. Peterson, S. Vyazovkin, C. a Wight, Macromol. Chem. Phys. 202 (2001) 775.
[51] A. Omrani, A.A. Rostami, F. Ravari, J. Therm. Anal. Calorim. 111 (2012) 677.
[52] R. Font, Thermochim. Acta 591 (2014) 81.
[53] A. Khawam, D.R. Flanagan, J. Phys. Chem. B 110 (2006) 17315.
[54] T. Hatakeyama, F.X. Quinn, Thermal Analysis: Fundamentals and Applications to Polymer Science, 2nd ed, second ed., John Wiley & Sons Ltd, West sussex PO191UD, England, 1999.
[55] L. Núñez, F. Fraga, M.R. Núñez, M. Villanueva, Polym. Guildf. 41 (2000) 4635.
[56] J.D. Badia, L. Santonja-Blasco, a Martínez-Felipe, a Ribes-Greus, Bioresour. Technol. 111 (2012) 468.
[57] P.E. Sánchez-Jiménez, L. a Pérez-Maqueda, A. Perejón, J.M. Criado, Polym. Degrad. Stab. 95 (2010) 733.
[58] P.E. Sánchez-Jiménez, L. a Pérez-Maqueda, A. Perejón, J.M. Criado, Polym. Degrad. Stab. 96 (2011) 974.
[59] R.E. Lyon, Thermochim. Acta 297 (1997) 117.
[60] E.S.P.B. V, E. Urbanovici, S.G. Branch, E. Segal, 168 (1990) 71.
[61] M. Salehi, F. Clemens, T. Graule, B. Grobéty, Appl. Energy 95 (2012) 147.
[62] M.E. Brown, M. Maciejewski, S. Vyazovkin, R. Nomen, J. Sempere, A. Burnham, 355 (2000).
[63] S. Vyazovkin, A.K. Burnham, J.M. Criado, L. a Pérez-Maqueda, C. Popescu, N. Sbirrazzuoli, Thermochim. Acta 520 (2011) 1.
[64] P. Budrugeac, E. Segal, L.A. Pérez-Maqueda, J.M. Criado, Polym. Degrad. Stab. 84 (2004) 311.
[65] M. Starink, Thermochim. Acta 288 (1996) 97.
[66] M. Starink, Thermochim. Acta 404 (2003) 163.
[67] S. Vyazovkin, 355 (2000).
[68] S. Vyazovkin, D. Dollimore, J. Chem. Inf. Model 36 (1996) 42.
[69] A. Berzins, A. Actins, Latv. J. Chem. (2012) 209.
[70] P. Budrugeac, Polym. Degrad. Stab. 89 (2005) 265.
[71] L. Fraga Grueiro, Estudio Cinético, Dinamomecánico Y Termogravimétrico Del Sistema Epoxídico BADGE n=0/m-XDA Mediante Las Técnicas de Análisis Térmico: DSC, DMA Y TGA, Construcción de Un Diagrama TTT, Universidade de Santiago de Compostela, 2001.
[72] F.J. Gotor, J.M. Criado, J. Malek, N. Koga, J. Phys. Chem. A 104 (2000) 10777.
[73] P. Budrugeac, J. Therm. Anal. Calorim. 89 (2007) 143.
[74] Z. Spitalsky, D. Tasis, K. Papagelis, C. Galiotis, Prog. Polym. Sci. 35 (2010) 357.
[75] P. Budrugeac, D. Homentcovschi, E. Segal, J. Therm. Anal. Calorim. 66 (2001) 557.
[76] S. Vyazovkin, N. Sbirrazzuoli, Anal. Chim. Acta 355 (1997) 175.
[77] P. Budrugeac, Thermochim. Acta 500 (2010) 30.
[78] J.M. Criado, P.E. Sánchez-Jiménez, L.A. Pérez-Maqueda, J. Therm. Anal. Calorim. 92 (2008) 199.
[79] A.R. Bhattacharyya, T. Sreekumar, T. Liu, S. Kumar, L.M. Ericson, R.H. Hauge, R.E. Smalley, Polym. Guildf. 44 (2003) 2373.
[80] V.G. Sister, E.M. Ivannikova, S.M. Lomakin, a. I. Yamchuk, Chem. Pet. Eng. 47 (2012) 741.
[81] P.E. Sánchez-Jiménez, L. a Pérez-Maqueda, A. Perejón, J.M. Criado, Resour. Conserv. Recycl 74 (2013) 75.
[82] P.E. Sánchez-Jiménez, L. a Pérez-Maqueda, A. Perejón, J.M. Criado, J. Phys. Chem. A 114 (2010) 7868.
[83] U. Hujuri, A.K. Ghoshal, S. Gumma, Waste Manag. 30 (2010) 814.
[84] M.S. Abbas-Abadi, M.N. Haghighi, H. Yeganeh, A.G. McDonald, J. Anal, Appl. Pyrolysis 109 (2014) 272.
[85] H. Wiener, J. Am, Chem. Soc. 69 (1947) 17.
[86] A. Aboulkas, K. El harfi, A. El Bouadili, Energy Convers. Manag. 51 (2010) 1363.
[87] P. Budrugeac, Thermochim. Acta 558 (2013) 67.
[88] F.S.M. Sinfrônio, J.C.O. Santos, L.G. Pereira, A.G. Souza, M.M. Conceição, V.J.F. Jr, V.M. Fonseca, 79 (2005) 393.
[89] P.E. Sánchez-Jiménez, L. a Pérez-Maqueda, A. Perejón, J.M. Criado, J. Phys. Chem. C 116 (2012) 11797.
[90] K.E. Strawhecker, E. Manias, Macromolecules 34 (2001) 8475.
[91] L. Nuñez, F. Fraga, M.R. Nuñez, M. Villanueva, J. Appl. Polym. Sci. 78 (2000) 1239.
[92] A. Marongiu, T. Faravelli, E. Ranzi, J. Anal. Appl. Pyrolysis 78 (2007) 343.
[93] C.L. Beyler, M.M. Hirschler, Quincy, MA, in: P.J. DiNenno (Ed.), SFPE, Handb. Fire Prot. Eng, second ed., 1995, pp. 1.110–1.131.
[94] A. Marcilla, A. Gómez-Siurana, D. Berenguer, Appl. Catal. A Gen. 301 (2006) 222.
[95] S. Turmanova, S. Genieva, L. Vlaev, J. Thermodyn. 2011 (2011) 1.
[96] M. Marinović-Cincović, B. Janković, V. Jovanović, S. Samaržija-Jovanović, G. Marković, Compos. Part B Eng. 45 (2013) 321.